JOURNAL OF SOLID STATE CHEMISTRY 105, 36–43 (1993)

Chemical State Analysis of Grain Boundaries in ZnO Varistors by Auger Electron Spectroscopy

SHIGERU TANAKA

Hitachi Ltd., 3-1-1 Saiwai-cho, Hitachi-shi, Ibaraki 317, Japan

CHIYOSHI AKITA

Taiyo Yuden Co., Ltd., 562 Hongo-Tsukanaka, Haruna-machi, Gunma-gun, Gunma 370-33, Japan

NAOKI OHASHI

Tokyo Institute of Technology, 2-12-1, O-okayama, Meguro-ku, Tokyo 152, Japan

JUN KAWAI

The Institute of Physical and Chemical Research, 2-1 Hirosawa, Wako-shi, Saitama 351-01, Japan

AND HAJIME HANEDA AND JUNZO TANAKA

National Institute for Research in Inorganic Materials, 1-1 Namiki, Tsukuba-shi, Ibaraki 305, Japan

Received June 2, 1992; in revised form November 4, 1992; accepted November 5, 1992

The chemical state of grain boundaries in Bi_2O_3-doped ZnO ceramics was investigated by Auger electron spectroscopy. The additive Bi was segregated into grain boundaries 2 to 3 nm thick, where oxygen deficiency occurred. Auger transitions $KL_{2,3}L_{2,3}$ for oxygen at the grain boundaries were composed of three peaks whose relative intensities varied with the amount of the segregated Bi. Results calculated using a molecular orbital method suggested that the metal–oxygen bonding state in the grain boundary changed with increased amounts of Bi. The change of the bonding character was considered to be related to the formation of an interfacial state at the grain boundary causing nonlinear current–voltage characteristics.

1. Introduction

Zinc oxide ceramics doped with a small amount of Bi show strongly nonlinear current–voltage (I–V) characteristics and are thereby widely used as varistors for surge absorption in various electric devices. The nonlinear I–V characteristics have been explained on the basis of the formation of a double Schottky-type potential barrier at the grain boundary (*1*).

It is known that the additive Bi has a decisive influence on the barrier formation and the other secondary additives such as Co and Mn improve the electrical properties of the ZnO varistor (*2*). For example, the figure of merit of the nonlinear characteristics ($\alpha = \log I/\log V$) is $\alpha = 1.5 \sim 5$ in a sample

0022-4596/93 $5.00

doped only with Bi_2O_3 and improves with further doping of cobalt oxide: $\alpha > 20$. However, the detailed origin of the nonlinear I–V characteristics has not been elucidated yet. To clarify the origin, it will be necessary to investigate the chemical state of the grain boundary.

As the scanning Auger electron spectroscopy (μ–AES) technique has high spatial resolution in the depth direction from a surface, it is applicable to the investigation of the chemical state of the grain boundary. We have tried AES measurements on a ZnO–Bi_2O_3 system and observed some spectroscopic variations. The results indicated that Bi-segregated layers existed at the grain boundary, causing oxygen deficiency, and that the Auger transition $KL_{2,3}L_{2,3}$ for oxygen varied depending on the amount of the segregated Bi. This paper reports on the chemical bonding state of the grain boundary in Bi_2O_3-doped ZnO varistors, including results calculated by a molecular orbital method.

2. Experimental

2.1 Sample Preparation

Two kinds of zinc oxide varistors, ZnO–0.5 mole% Bi_2O_3 (denoted as ZB05) and ZnO–1.0 mole% Bi_2O_3 (ZB10), were prepared. Starting powders were synthesized by a coprecipitation method (*3*). A mixed solution of $ZnCl_2$ and $BiCl_3$ was added to 1 *N* diethylamine solution to coprecipitate hydroxides of Zn and Bi. The powders were calcined at 550°C for 5 hr in air and then pressed into cylindrical shape (3 mm in diameter and 40 mm in length) under 400 MPa of cold isostatic pressure. The rods were fired at 1200°C for 1 hr in air. Grain size of the samples ranged from 10 to 20 μm. Pelletized specimens (8 mm in diameter and 1 mm in thickness) were prepared for measurements of I–V characteristics in the same way.

Standard samples for quantitative μ–AES analysis, i.e., Bi_2O_3 and pure ZnO, were prepared by firing in air at 550°C for 2 hr and at 1200°C for 1 hr, respectively.

2.2 Measurements

Electrical properties were measured at room temperature by a two-probe method using indium–gallium alloy electrodes. Both ZB05 and ZB10 showed nonlinear I–V characteristics; α-value was about 1.8.

μ-AES was carried out by a high energy-resolution AES system (VG Microlab 320-D). The cylindrical samples were fractured in the ultra-high-vacuum chambers (3×10^{-8} Pa) of the system and measured as soon as possible to avoid surface pollution. The samples fractured mostly along the grain boundaries. An accelerating voltage of electron beam was 5 kV. The beam diameter was about 300 nm, which was small enough in comparison with the grain size.

Depth profiles were obtained by alternating μ-AES measurement and sputtering the fractured surface with an Ar-ion beam. The accelerating voltage of the ion beam was 3 kV with a current of 600 nA. An etching rate was approximately 0.03 nm/sec. Quantitative analysis was performed using relative sensitivity factors (RSFs) estimated from peak heights of derivative spectra of the standard samples.

3. Results

Figure 1 shows a derivative AES spectrum obtained from a fractured surface (i.e., grain boundary) of ZB10. Auger transition *LMM* for Zn was observed near 1000 eV, *KLL* for O near 500 eV, and *NVV* for the additive Bi near 100 eV. The Auger signal of Bi was observed at all of the grain boundaries in the present samples.

Figure 2A shows typical *NVV* transitions for Bi observed at three different grain boundaries. The content of Bi varied with grain boundaries. Figure 2B shows the corresponding $KL_{2,3}L_{2,3}$ transitions of O. The three lines are normalized to coincide with

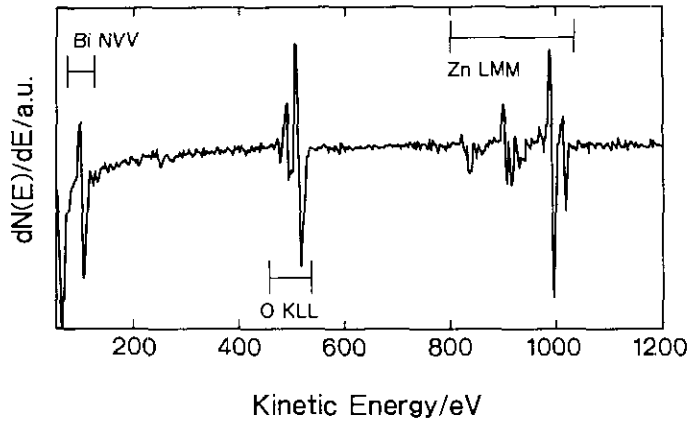

FIG. 1. A derivative Auger electron spectrum of the grain boundary in a Bi_2O_3-doped ZnO ceramic. The sample was fractured under 3×10^{-8} Pa.

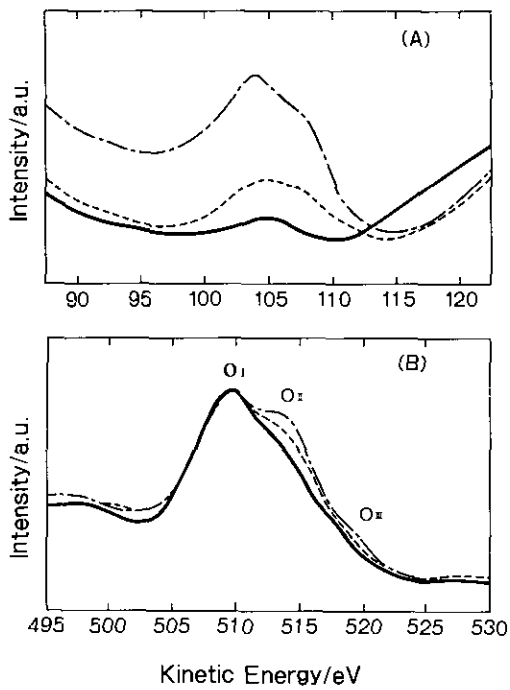

FIG. 2. Auger electron spectra observed at three different grain boundaries: (A) *NVV* transition for Bi and (B) $KL_{2,3}L_{2,3}$ transition for O. The same types of lines in (A) and (B) indicate the spectra obtained at the same points.

the intensity of the O_I peak. The $KL_{2,3}L_{2,3}$ transition was composed of two peaks (O_I: 510 eV, O_{II}: 514 eV) at grain boundaries with a small amount of Bi (solid line) and three peaks (O_I: 510 eV, O_{II}: 514 eV, O_{III}: 518 eV) at grain boundaries with a relatively large amount of Bi (dashed lines). In particular, the intensity of the O_{II} and O_{III} peaks increased with increased Bi content. The $KL_{2,3}L_{2,3}$ transition for O of the Bi-poor grain boundary (solid line in Fig. 2B) was similar to that of a pure ZnO sample.

To quantify the AES spectra, the relative sensitivity factors of Bi and Zn to O were determined by averaging values of five different points of the standard Bi_2O_3 and pure ZnO. The averaged values were 1.7 for Bi and 1.4 for Zn. The accelerating voltage and current of the electron beam were fixed for the quantitative analysis. The accuracy of the RSFs was within about 10%; this scatter of RSF was considered to be due to the difference of crystal directions of the fractured surface and/or to surface irregularity.

Figure 3 shows a relation between Bi and O contents observed at many grain boundaries in ZB05(×) and ZB10(○). The data on the left axis were obtained from pure ZnO. The O content decreased with increased Bi content.

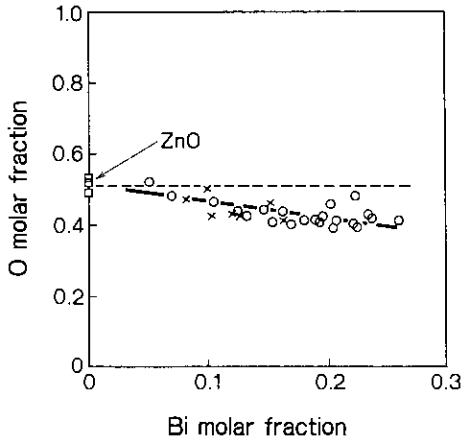

FIG. 3. Relation between Bi and O content observed at many grain boundaries of Bi_2O_3-doped ZnO ceramics.

Figure 4 illustrates a depth profile at the grain boundary of ZB05. The vertical axis is the molar fraction and the horizontal axis is the etching time by an Ar-ion beam; the left end of the data corresponds to the fractured surface. The additive Bi was segregated into a grain boundary 2 to 3 nm thick, where Zn and O content decreased. It is noteworthy that the ratio of Zn to O was almost constant (about 1) at the intragrain and even at the grain boundary: this ratio seems to be independent of the amount of the segregated Bi. In other words, the total amount of cations (Zn + Bi) was higher than that of the anion (O) at the grain boundary (*4*). This behavior was also observed in ZB10.

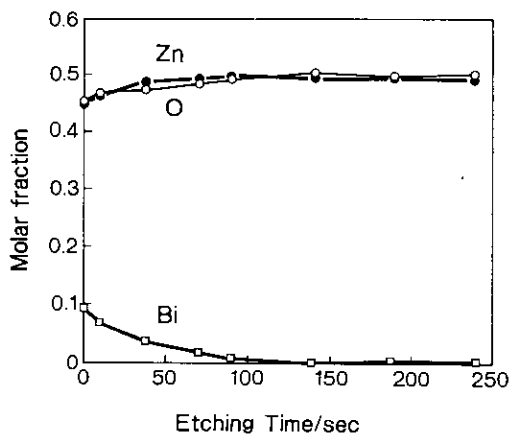

FIG. 4. Depth profile near the grain boundary of ZnO–0.5 mol% Bi_2O_3.

4. Discussion

4.1 Chemical Effect of Bi at the Grain Boundary

The additive Bi is highly segregated at the grain boundary in spite of the small doping amount. Considering that a simple chemical reaction between bismuth oxide and zinc oxide occurs at the grain boundary, the possible chemical form of bismuth oxide is thought to be either of the following types:

(1) stoichiometric bismuth oxide, i.e., Bi_2O_3, or

(2) bismuth oxide with some amount of oxygen deficiency, i.e., $BiO_{1-\delta}$.

Figure 5 shows the schematic dependence of the O content upon the Bi content in the respective types of bismuth oxide. The line (B) in Fig. 5 corresponds to $\delta = 0$ in case (2) and the line (C) to $\delta > 0$. The comparison of Figs. 3 and 5 indicates that the experimental result qualitatively agrees with line (C); i.e., $\delta > 0$ in case (2). Thus, it is considered that the segregation of Bi results in the production of oxygen deficiencies at the grain boundaries.

As shown in Fig. 4, the depth profile indicates that the O content in the Bi-segregated region is less than the total content of the metallic elements (*4*). This also supports the conclusion that the segregated Bi ions cause oxygen deficiencies at the grain boundaries. Taking into account the difference of ionic radii (*5*) between Zn (0.07 nm) and Bi (0.11 nm), it is possible to consider that large Bi ions can enter the Zn site by producing the oxygen vacancy needed to maintain a structural skeleton of ZnO.

The existence of the oxygen deficiencies was also observed for samples that did not show the nonlinear *I–V* characteristics (i.e.,

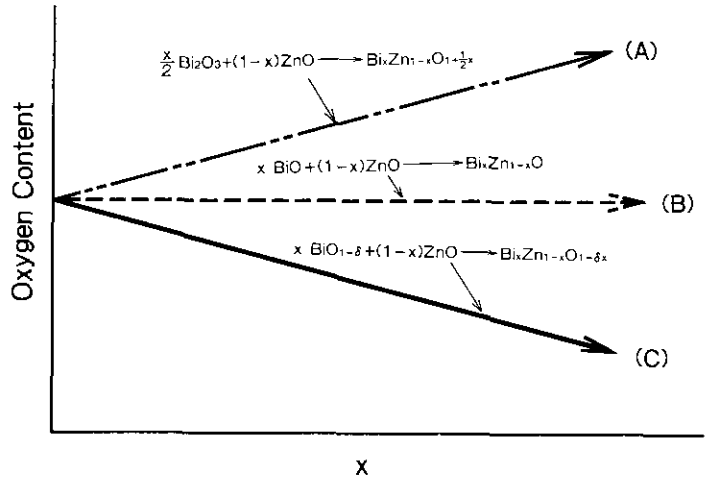

FIG. 5. Schematic relations between O and Bi content for possible chemical reactions at grain boundaries in Bi_2O_3-doped ZnO ceramics.

samples annealed in nitrogen gas). In addition, we could not observe any obvious difference in the chemical content at the grain boundary between the samples with and without the nonlinear I–V characteristics. As the density of interfacial states in ZnO varistors is in general $N_i = 2 \times 10^{12}$ to $10^{13}/cm^2$ (*6*) and the surface atomic density of ZnO is about $10^{15}/cm^2$, content changes of Zn and O at the grain boundary accompanied by the introduction of the interfacial states, if they occur, are expected to be less than 1%. Thus, the difference in the chemical content at the grain boundary between these two type of samples is too small to be clearly detected by the AES technique.

Greuter *et al.* (*7, 8*) reported that the change of oxygen content corresponding to the α-value could be observed by X-ray photoelectron spectroscopy (XPS) and AES techniques for commercial ZnO varistors with more complicated compositions. Their results might suggest the possibility that secondary additives such as Co and Mn vary the chemical state of the grain boundaries.

4.2 Bonding State of Oxygen 2p-Orbital

As shown in Fig. 2, the Auger transition $KL_{2,3}L_{2,3}$ for O is composed of two or three peaks. Weisz *et al.* (*9*) also observed similar shoulder peaks for a single crystal of ZnO. The enhancement of the intensities of the O_{II} and O_{III} peaks due to the segregation of Bi suggests that the bonding state of the oxygen valence orbital is perturbed by Bi.

To analyze these AES spectra, a discrete-variational (DV)–$X\alpha$ method (*10, 11*) was applied to a $[Zn_4O]^{6+}$ cluster (distorted tetrahedral structure) shown in Fig. 6. This cluster belongs to the C_{3v} symmetry. Atomic distances between a centered oxygen and coordinated zinc atoms are given in Fig. 6.

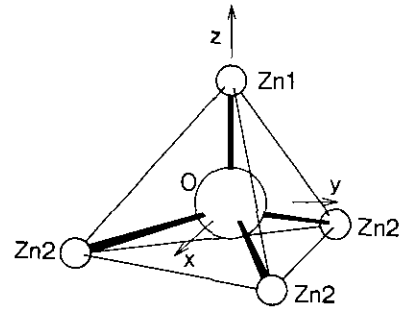

$r_0(O-Zn1) = 0.179\ nm$
$r_0(O-Zn2) = 0.203\ nm$

FIG. 6. Structure of the $[Zn_4O]$ cluster. r_0 is the bonding length after Ref. (*16*).

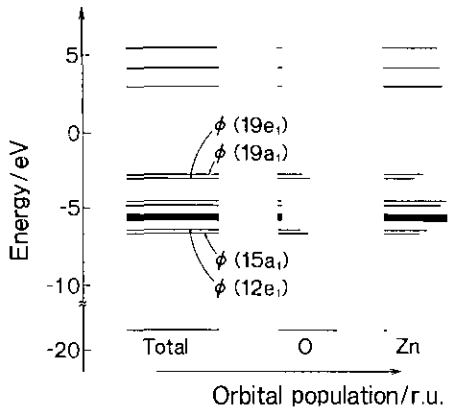

FIG. 7. Energy levels of molecular orbitals in the vicinity of the valence band and their partial densities of the states of O_{2p} and Zn_{3d}.

According to the DV–$X\alpha$ calculation, the O $2p$-orbital contributes primarily to the four molecular orbitals $\Phi(15a_1)$, $\Phi(12e_1)$, $\Phi(19e_1)$, and $\Phi(19a_1)$, which combine with the surrounding Zn $3d$- and $4s$-orbitals. As shown in Fig. 7, the molecular orbitals $\Phi(15a_1)$ and $\Phi(12e_1)$ are located at nearly the same energy, 6 eV below a midpoint of band gap (E_0) (hereafter, they are denoted by $\Phi(E_L)$), and $\Phi(19e_1)$ and $\Phi(19a_1)$ are located above $\Phi(15a_1)$ and $\Phi(12e_1)$, 3 eV below E_0 (denoted by $\Phi(E_U)$). The orbitals $\Phi(12e_1)$ and $\Phi(19e_1)$ are doubly degenerate, occupied by four electrons, and the orbitals $\Phi(15a_1)$ and $\Phi(19a_1)$ are nondegenerate, occupied by two electrons. $\Phi(19a_1)$ is the highest occupied molecular orbital (HOMO).

Figure 7 also gives the local and partial electron density of state (DOS) of each molecular orbital. In this figure, the length of the horizontal bars is relatively proportional to the partial DOS of each element (O and Zn). AES transitions occur between these energy states (orbitals); therefore, 16 O $KL_{2,3}L_{2,3}$ transitions are possible.

Auger transition probability I_{KXY} is given by a self-convolution of local and partial DOS (*12, 13*); therefore, I_{KXY} is calculated from Fig. 7. The calculated AES spectrum of oxygen $KL_{2,3}L_{2,3}$ is illustrated in Fig. 8. In this figure, we denote, for example, a transition in which one electron in the $\Phi(E_L)$ orbital falls into the core hole of an internal orbital (O_{1s}) and then another electron in the $\Phi(E_U)$ orbital is ejected as an Auger electron by $\Phi(E_L)/\Phi(E_U)$: the other transitions are similarly denoted. Here, the full width at half maximum of DOS was assumed to be 3 eV for every energy level. The detailed treatments and results of the DV–$X\alpha$ calculation will be published elsewhere in the near future (*14*).

Comparing the calculated spectrum to those observed for pure ZnO and for the grain boundary with the small amount of segregated Bi, both energy differences and peak ratios are in good agreement. From the DV–$X\alpha$ calculation, the peaks O_I, O_{II}, and O_{III} in Fig. 2B can be identified with the AES transitions $\Phi(E_L)/\Phi(E_L)$, $\Phi(E_L)/\Phi(E_U)$, and $\Phi(E_U)/\Phi(E_U)$, respectively.

Figure 9 shows contour plots of $\phi(15a_1)$ and $\Phi(19a_1)$. Here, solid and dashed lines mean plus and minus parts of each molecular orbital, respectively. From this figure, it is seen that the energy level of $\Phi(15a_1)$ mainly consists of bonding orbitals of O_{2p} and Zn_{3d}, while $\Phi(19a_1)$ contains a partially antibonding π-component.

As mentioned above, the Auger transition probability reflects the partial DOS of a molecular orbital, namely, the bonding character. The growth of the intensities of O_{II} and O_{III} due to the Bi-segregation means that the contribution of the O_{2p} orbital to the higher energy molecular orbitals $\Phi(19e_1)$ and $\Phi(19a_1)$ becomes larger with increasing Bi content. That is, the partial DOS of O is decreased in $\Phi(E_L)$ and increased in $\Phi(E_U)$ by the segregation of Bi.

Further discussion is somewhat speculative but plausible within the scope of this study. It is known that frontier electron theory is very useful in understanding chemical reactions in organic materials. According to this theory, HOMO and LUMO (lowest unoccupied molecular orbital) play an important role in the chemical reaction. As mentioned above, HOMO in the ZnO grain

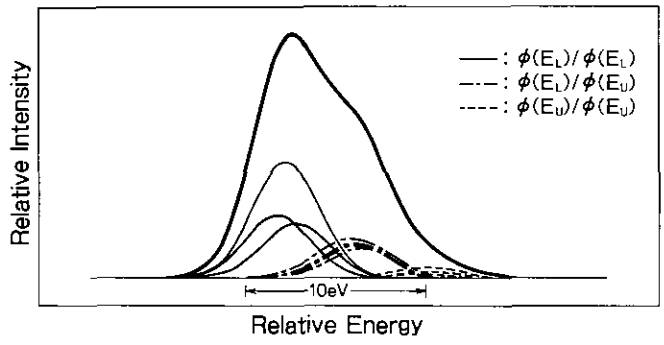

FIG. 8. An Auger $KL_{2,3}L_{2,3}$ spectrum calculated for O in a $[Zn_4O]^{6+}$ cluster by DV–$X\alpha$ method. Sixteen transitions are possible for the $KL_{2,3}L_{2,3}$ transition. Notations in the figure are described in the text.

boundary is rearranged by the segregation of Bi, and it is known that doping with a slight amount of Bi is very effective in producing nonlinear I–V characteristics in the ZnO varistor. It is therefore conjectured that the change of the bonding character due to the Bi segregation enhances the formation and/or chemical stability of adherent molecules (possibly oxygen (*15*)) at the grain boundaries. Such adherent molecules probably act as interfacial states, resulting in the formation of interfacial potential barriers in the ZnO–Bi_2O_3 system by firing in air.

5. Conclusions

The chemical state of the grain boundaries in the ZnO–Bi_2O_3 system was investigated by the μ–AES technique. The additive Bi ions were segregated into grain boundaries 2 to 3 nm thick, causing oxygen deficiencies. The Auger transition $KL_{2,3}L_{2,3}$ for O varied

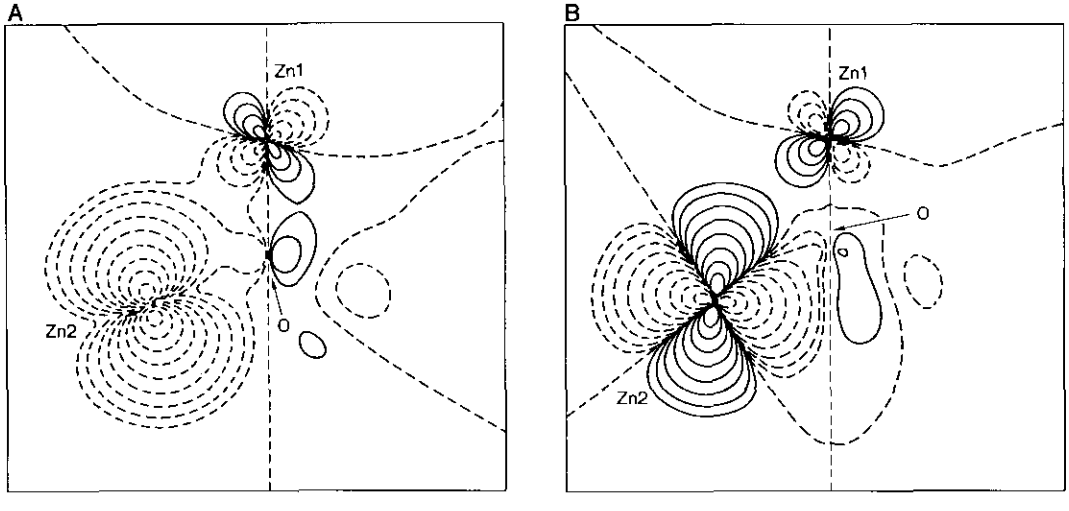

FIG. 9. Contour plots of two molecular orbitals, (A) $\Phi(15a_1)$ and (B) $\Phi(19a_1)$.

with the amount of the segregated Bi, which indicated that the metal–oxygen chemical bonding state at the grain boundary changes corresponding to the amount of the segregated Bi. These results suggested that the stability of interfacial states or the formation of the potential barrier was related to the chemical bonding state at the grain boundaries.

Acknowledgments

The authors thank Drs. T. Miyoshi, K. Maeda, and K. Takahashi of Hitachi Res. Lab., Hitachi, Ltd., Dr. M. Fujimoto of Taiyo Yuden Co., Ltd., and Dr. S. Hishita of NIRIM for valuable discussions and encouragement during this work. This work was supported by Special Coordination Funds for Promoting Science and Technology of S.T.A. Japan (Project of "Elementary Function of Materials").

References

1. G. Blatter and F. Greuter, *Phys. Rev. B* **33** (6), 3952 (1986).
2. M. Matsuoka, *Jpn. J. Appl. Phys.* **10** (6), 736 (1971).
3. S. Hishita, Y. Yao, and S. Shirasaki, *J. Am. Ceram. Soc.* **72** (2), 338 (1989).
4. J. Tanaka, H. Haneda, S. Hishita, F. P. Okamura, and S. Shirasaki, *J. Phys. C* **51** (1), 1055 (1990).
5. R. D. Shannon, *Acta Crystallogr. Sect. A* **32,** 751 (1976).
6. K. Sato, J. Tanaka, H. Haneda, A. Watanabe, and S. Shirasaki, *J. Ceram. Soc. Jpn. Int. Ed.* **97** (10), 1228 (1989).
7. F. Greuter, G. Blatter, M. Rossinelli, and F. Stucki, *in* "Advances in Varistor Technology," (L. M. Levinson, Ed.), p. 31, Amer. Ceramic Soc. (1989).
8. F. Stucki, P. Bruesch, and F. Greuter, *Surf. Sci.* **189/190,** 294 (1987).
9. S. Z. Weisz, O. Resto, Y. Goldstein, G. Yaron, and A. Many, *J. Vac. Sci. Technol. A* **6** (5), 3012 (1988).
10. D. E. Ellis and G. S. Painter, *Phys. Rev. B* **2** (8), 2887 (1970).
11. H. Adachi, M. Tsukada, and C. Satoko, *J. Phys. Soc. Jpn.* **45** (3), 875 (1978).
12. D. E. Ramaker, J. S. Murday, N. H. Turner, G. Moore, M. G. Lagally, and J. Houston, *Phys. Rev. B* **19** (10), 5375 (1979).
13. J. Ghijsen, L. H. Tjeng, J. van Elp, H. Eskes, J. Westerink, G. A. Sawatzky and M. T. Czyzyk, *Phys. Rev. B* **38** (16), 322 (1988).
14. J. Tanaka *et al.*, in preparation.
15. T. K. Gupta and W. G. Carlson, *J. Mater. Sci.* **20,** 3487 (1985).
16. R. W. G. Wyckoff, "Crystal Structures," Vol. 1, p. 111, Interscience, New York (1965).